Cochlear outer hair cell horizontal top connectors mediate mature stereocilia bundle mechanics

Alexander X Cartagena-Rivera, Sébastien Le Gal, Kerianne Richards, Elisabeth Verpy, Richard S Chadwick

BIOPHYSICS

Cochlear outer hair cell horizontal top connectors mediate mature stereocilia bundle mechanics

Alexander X. Cartagena-Rivera[1]*, Sébastien Le Gal[2,3,4], Kerianne Richards[5], Elisabeth Verpy[2,3,4], Richard S. Chadwick[1]*

Outer hair cell (OHC) stereocilia bundle deflection opens mechanoelectrical transduction channels at the tips of the stereocilia from the middle and short rows, while bundle cohesion is maintained owing to the presence of horizontal top connectors. Here, we used a quantitative noncontact atomic force microscopy method to investigate stereocilia bundle stiffness and damping, when stimulated at acoustic frequencies and nanometer distances from the bundle. Stereocilia bundle mechanics were determined in stereocilin-deficient mice lacking top connectors and with detached tectorial membrane (*Strc*$^{-/-}$/*Tecta*$^{-/-}$ double knockout) and heterozygous littermate controls (*Strc*$^{+/-}$/*Tecta*$^{-/-}$). A substantial decrease in bundle stiffness and damping by ~60 and ~74% on postnatal days P13 to P15 was observed when top connectors were absent. Additionally, we followed bundle mechanics during OHC top connectors development between P9 and P15 and quantified the observed increase in OHC bundle stiffness and damping in *Strc*$^{+/-}$/*Tecta*$^{-/-}$ mice while no significant change was detected in *Strc*$^{-/-}$/*Tecta*$^{-/-}$ animals.

INTRODUCTION

Sensory hair cells of the inner ear are active mechanosensitive machines that transform sound-induced mechanical vibrations into electrical signals (*1*). The sensory epithelium of the cochlea, the organ of Corti, has two types of sensory hair cells, the inner and outer hair cells (IHCs and OHCs, respectively). IHCs are genuine sensory cells that transmit information via the cochlear nerve fibers to the brainstem auditory nuclei (*2*). In contrast, OHCs, which are endowed with electromotility, constitute the cochlear amplifiers that contribute to the detection of weak sound-induced vibrations (*3*, *4*). The organ of Corti sensory epithelium is positioned between a sheet of paucicellular connective tissue, the basilar membrane, and an acellular gel, the tectorial membrane (TM). Sound-induced vibrations of the basilar and tectorial membranes stimulate the mechanosensitive sensory cells' stereocilia bundles. The mammalian stereocilia hair bundles of OHCs are arranged in three rows of graded height and are tightly interconnected. The tallest row is embedded into the tectorial membrane. As a result, the OHCs are stimulated by displacements of the tectorial membrane relative to the reticular lamina (the apical surface of the organ of Corti). In contrast, the IHC stereocilia bundle is freestanding and is stimulated by the motion of the endolymphatic fluid. Deflection of the stereociliary hair bundle opens tension-gated ion channels located at the tips of stereocilia from the short and middle rows, which produces a receptor potential in the sensory hair cell.

The forces felt by the stereocilia hair bundle are transmitted to mechanoelectrical transduction (MET) channels. The cooperative way MET channels open during bundle deflection depends critically on the cohesiveness of the hair bundle (*5*, *6*), where adjacent stereocilia are grouped and interconnected by tip links (*7*), transient lateral links (*8*), transient ankle links (*9*), and zipper-like horizontal top connectors (*10*, *11*) that are specific to OHCs. The latter links connect adjacent stereocilia both within and across stereocilia rows and are thought to be a major contributor to the maintenance of OHC hair bundle cohesion at mature stages (*11*). The top connectors are thought to have two essential functions: (i) the maintenance of bundle-cohesive architecture by bundling the stereocilia together to form a cohesive V-shape structure to minimize frictional drag and (ii) keeping the bundle as a coherent unit when moving dynamically (*5*, *6*, *11*). Deflection of the stereocilia bundle results in coordinated mechanical opening or closing of MET channels at the tip of the stereocilia of the short and middle rows. Possible mechanical mechanisms involving the action of top connectors include (i) generation of tension or compression in extensible horizontal top connectors, (ii) enabling sliding adhesion with inextensible top connectors, or (iii) a combination of both mechanisms (*5*). Nevertheless, it is poorly understood how the hair cell bundle mechanical properties are related and regulated by specific molecular structures such as intersterocilia links to achieve controlled sensory cellular processes. Here, we directly assess the mechanical contribution of the cohesive architecture of the hair bundle by measuring the passive stiffness and damping of bundles with and without horizontal top connectors.

Stereocilin is the protein defective in the human deafness nonsyndromic DFNB16 (*12*). In mice, this protein has been shown to be associated with the OHC horizontal top connectors and the tectorial membrane attachment crowns located at the apex of the tallest stereocilia row (*13*, *14*). Stereocilin-deficient mice (*Strc*$^{tm1Ugds/tm1Udgs}$, referred to as *Strc*$^{-/-}$), exhibit progressive hearing loss beginning at postnatal age 15 (P15). *Strc*$^{-/-}$ mice lack horizontal top connectors and tectorial membrane attachment crowns, but their OHC hair bundles are still stimulated by the tectorial membrane periodic motion (*13*, *14*). In addition, the *Strc*$^{-/-}$ mice from P14 lack distortion product otoacoustic emissions, a hallmark of normal OHC function (*13*), as well as electrical distortion and suppressive masking. However, during a few days after the onset of hearing (at P14), the cochlear sensitivity and frequency tuning in these mice are almost intact (*13*). Several hypotheses have been suggested to explain the lack of generation of distortions in the presence of persisting MET in these mice (*13*, *15*). The unique phenotype of *Strc*$^{-/-}$ mice suggests that the main source of cochlear

[1]Section on Auditory Mechanics, National Institute on Deafness and Other Communication Disorders, National Institutes of Health, Bethesda, MD 20892, USA. [2]Unité de Génétique et Physiologie de l'Audition, Institut Pasteur, 75015 Paris, France. [3]UMRS 1120, Institut National de la Santé et de la Recherche Médicale (INSERM), 75015 Paris, France. [4]Sorbonne Universités, Université Pierre et Marie Curie Paris 06, Complexité du Vivant, 75005 Paris, France. [5]Genomics and Computational Biology Core, National Institute on Deafness and Other Communication Disorders, National Institutes of Health, Bethesda, MD 20892, USA.
*Corresponding author. Email: alexander.cartagena-rivera@nih.gov (A.X.C.-R.); chadwick@helix.nih.gov (R.S.C.)

waveform distortions is top connector–mediated MET channel cooperativity, i.e., the coordinated opening of MET channels induced by the synchronous motion of all stereocilia interconnected by horizontal top connectors. An alternative explanation would be that the top connectors have biophysical properties that are capable of conferring nonlinear stiffness on the OHC hair bundle (*15*, *16*). For example, horizontal top connectors would be tight when the hair bundle is deflected in the excitatory direction and relaxed in the inhibitory direction (*13*, *15*).

The mechanical properties of OHC and IHC stereociliary bundles are crucial to better understand the mechanics of hearing. Since the primary physical parameter contributing to mechanical coherence of OHCs is the effective stereocilia bundle normal stiffness, many experimental methods have been used to determine it. Stiff microprobes for bundle deflection in the excitatory/inhibitory direction (*17*, *18*) are the most commonly used methodology to measure the stereocilia hair bundle stiffness. Despite its historical value, use of stiff microprobes has critical limitations: (i) they are unable to stimulate the bundle at physiological frequencies (kHz), (ii) the contact between the probe and the hair bundle is unevenly distributed, and (iii) large forces (hundreds of piconewtons to nanonewtons) are required for optical detection of bundle deflection, potentially disrupting the hair bundle and causing splaying. The fluid jet stimulation method (*19*, *20*) overcomes some of these limitations but is still unable to stimulate the bundle with physiological relevant acoustic frequencies, and more importantly, the extraction of quantitative stiffness values has proven difficult to achieve. Therefore, the development of a new method to more accurately measure hair bundle passive elastic stiffness and viscous damping under conditions relevant to hearing is needed. Note that no method has been able to measure the sensory stereocilia bundle viscous damping parameter in mice with high sensitivity. The experimental determination of the bundle viscous damping parameter is important for understanding cochlear amplification, since the viscous drag by the surrounding fluid and the viscoelasticity of stereociliary connecting links damp the bundle and limit cochlear amplification (*21*, *22*). Last, previous studies aimed at measuring OHC bundle stiffness in mice were limited to early postnatal ages (P0 to P7) before the formation and development of top connectors (*23*). No measurements were performed on more mature ages when the bundle is anchored into the tectorial membrane (P9 onward) and thus potentially damaged when it is peeled off before recordings.

Here, we describe the use of noncontact acoustic frequency modulation atomic force microscopy (FM-AFM) (*24*, *25*) to determine the hair bundle passive stiffness and damping (dominated by the component normal to the stereocilia bundle; Fig. 1) with a more physiological stimulus relevant to hearing. This noncontact method is based on the phenomenon that, when a micrometer-sized bead attached to an AFM cantilever vibrating at acoustic frequencies in a fluid medium is brought near the sample surface, from micrometers to within nanometer distances of the target, a hydrodynamic coupling interaction between the fluid and sample causes a frequency shift to the bead motion that can be easily measured with a sensitive AFM detection system. To calculate the hair bundle passive mechanics, we developed a mathematical model to relate frequency shifts in the bead displacement to bundle stiffness and viscous damping (Eqs. 1 and 2). Moreover, to minimize hair bundle damage caused by peeling off of the tectorial membrane, we used animals with a constitutively detached tectorial membrane by generating a stereocilin and α-tectorin ($Tecta^{\Delta ENT/\Delta ENT}$ referred to as $Tecta^{-/-}$) (*26*) double-knockout mice to compare bundle mechanics with and without the horizontal top connectors.

Using the noncontact FM-AFM method, we found that the absence of horizontal top connectors in apical turn cochlear OHCs leads to a marked reduction of hair bundle passive stiffness by ~60%, suggesting that top connectors are a dominant contributor to mature OHC bundle stiffness. In addition, we observed that hair bundles are viscoelastic and that the absence of top connectors in OHCs significantly reduces the passive bundle damping parameter. Last, by tracking the developmental changes of OHC stereocilia bundle stiffness during the period (P9 to P15) encompassing the development of top connectors (*11*), we found a much larger increase in hair bundle stiffness in $Strc^{+/-}/Tecta^{-/-}$ mice than in $Strc^{-/-}/Tecta^{-/-}$ mice, confirming that, at late postnatal stages of OHC development, bundle stiffness is dominated by the maturation of horizontal top connectors. Together, these results show that horizontal top connectors are major contributors to OHC mature bundle mechanics.

RESULTS

Theory to determine the stereocilia hair bundle stiffness from frequency shifts in the bead oscillation

A hair bundle stiffness–frequency shift relationship has been developed here to determine the stiffness of a deformable hair bundle protruding from the apical cuticular plate of a hair cell. Consider a micrometer-sized rigid sphere attached to the end of a microcantilever with a calibrated spring constant oscillating at acoustic frequencies (kHz) with nanometer oscillation amplitude in an incompressible fluid bath (Fig. 1B). When close to a hair bundle, the up-and-down motion of the sphere at acoustic frequencies induces fluid movements with normal and axial components that are close to the physiological stimulation of the bundle by sound (*27*). As the oscillating sphere approaches to within nanometers of the stereocilia bundle, a frequency shift will occur. An important assumption is that the sphere oscillation amplitude (5 nm) is small compared to the minimum gap height, which is set to be 50 nm, which, in turn, is small compared to the sphere radius (5 μm) (*24*, *25*, *28*). Another critical assumption, not used in previous studies (*24*, *25*, *28*), is that the surface of the sensory epithelium is inclined to the basilar membrane by the angle β (hereafter referred to as the sensory epithelium angle; Fig. 1B), and this effect breaks symmetry; thus, the basic fluid flow is not axisymmetric. The fluid flow in the gap is driven by the velocity of the oscillating sphere, which has an axisymmetric flow component $V\cos\beta$ normal to the reticular lamina and a nonaxisymmetric flow $V\sin\beta$ tangent to it. The normal component at small β angles (≤15° for conditions in present study) dominates the stimulation compared to the more complicated tangential component. The analytical formula that describes the relationship between frequency shift and the hair bundle stiffness component normal to the tallest stereocilia is

$$k_b = 2k_c^{\frac{2}{3}}\Delta f^{\frac{2}{3}}\left(\frac{3\mu}{\pi R f_{far}}\right)^{\frac{1}{3}}\left(\frac{A_b\sin\beta}{\left(h_m^2\left(\frac{h_{far}}{h_m}-1\right)\cos\beta\right)^{\frac{2}{3}}}\right) \quad (1)$$

where k_b (N m^{-1}) is the hair bundle stiffness, k_c (N m^{-1}) is the calibrated cantilever spring constant, μ (Pa·s) is the incompressible fluid viscosity, β (rad) is the sensory epithelium angle (the angle between the basilar membrane and the reticular lamina), A_b is the effective area at the

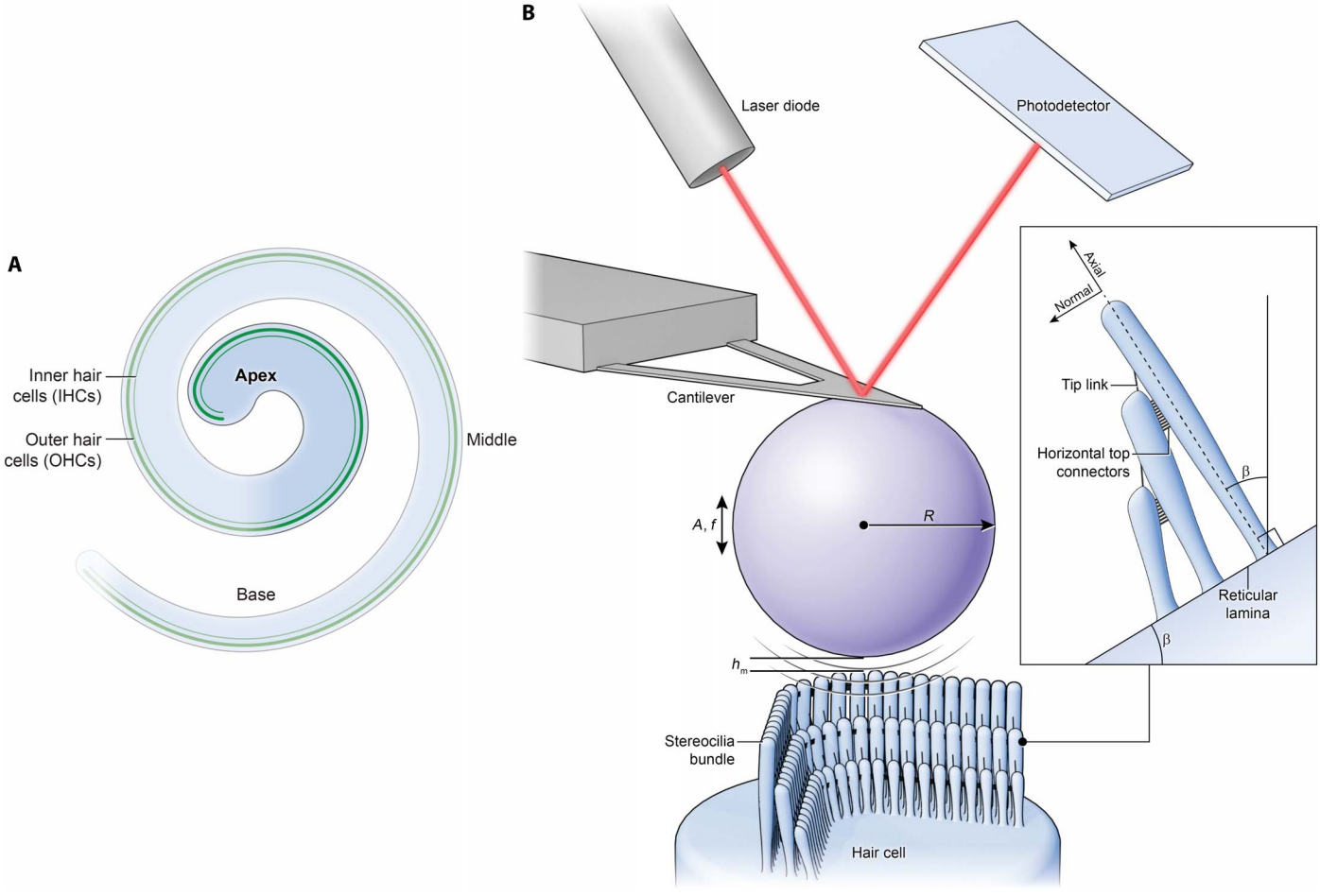

Fig. 1. Noncontact acoustic FM-AFM for quantitative and physiological measurement of stereociliary bundle mechanical properties. (**A**) The schematic illustrates the organ of Corti subdivided into three regions: base, middle, and apex. Sensory hair cells (three OHC rows and one IHC row) are illustrated in green. The highlighted apical turn region is the location where all experiments were performed. (**B**) The diagram illustrates the noncontact acoustic FM-AFM method to measure the stereociliary hair bundle stiffness of OHCs and IHCs. It is based on the phenomenon that, when an acoustically vibrating AFM cantilever with an attached micrometer-sized bead in a liquid environment approaches within nanometer distances from the sample surface, a hydrodynamic coupling interaction will cause a frequency shift (Δf) to the cantilever oscillation that can be easily measured with the sensitive AFM detection (laser diode and photodetector) system. The photodetector records the displacement of the AFM cantilever with nanometer sensitivity. In the diagram, A is the oscillation amplitude, f is the cantilever/bead drive frequency, R is the microbead radius, h_m is the minimum gap height, and β is the angle between the reticular lamina and the basilar membrane.

top of the bundle, R (m) is the sphere radius, h_m (m) is the minimum gap height or distance between the sphere and the tallest stereocilia row, h_{far} (m) is the farthest distance between the sphere and the tallest stereocilia row when the cantilever dynamics are unperturbed, $\Delta f = f_{near} - f_{far}$ (Hz) is the frequency shift of the bead oscillation when the vibrating microsphere is moved closer to the stereocilia bundle where the phase is $\pi/2$, f_{far} (Hz) is the unperturbed resonant frequency of the cantilever vibrating far from the bundle when the phase is $\pi/2$, and f_{near} (Hz) is the perturbed resonant frequency of the cantilever vibrating to within-nanometer distance away from the bundle when the phase is $\pi/2$. The "Phase" is defined as the phase lag between the reference phase of the piezo vibration and the phase of the AFM cantilever with the attached bead. See section S1 for theoretical development.

We also determined the stiffness of a soft tipless cantilever using a variation of Eq. 1. We precalibrated tipless, triangular, silicon nitride Bruker MLCT AFM microcantilevers using the thermal tune method (*29*) built into the Catalyst AFM system. The calibrated stiffness was $k_{thermal} = 45.7 \pm 2.3$ pN nm^{-1} (mean ± SEM). Then, we used the cantilever with a 10-μm bead attached and recorded frequency sweeps at different distances around the resonance frequency $f_{\pi/2}$, where the phase was set to $\pi/2$ at a distance of 1 μm (Fig. 2A). In Fig. 2B, it can be observed that as the vibrating cantilever with a microbead was moved closer from 1 μm to within 50 nm from the calibrated tipless cantilever, the frequency $f_{\pi/2}$ shifted to higher frequencies due to an increase in the strength of the hydrodynamic interaction forces. We then used Eq. 1, with the effective area $A_{eff} = A_b \sin\beta = 4\pi R h_m$, to determine the tipless cantilever spring constant and obtained values $k = 58.1 \pm 5.5$ pN nm^{-1} (Fig. 2C). The fact that this value obtained using noncontact FM-AFM is comparable to and is not significantly different ($P = 0.14$; Fig. 2C) from the precalibrated values by the standard thermal noise fluctuations method confirmed the ability of our method to measure sample stiffness.

Applied force to hair bundles

We then computed the amount of force applied to stimulate the stereocilia hair bundle through the fluid-structure coupling. Fluid coupling

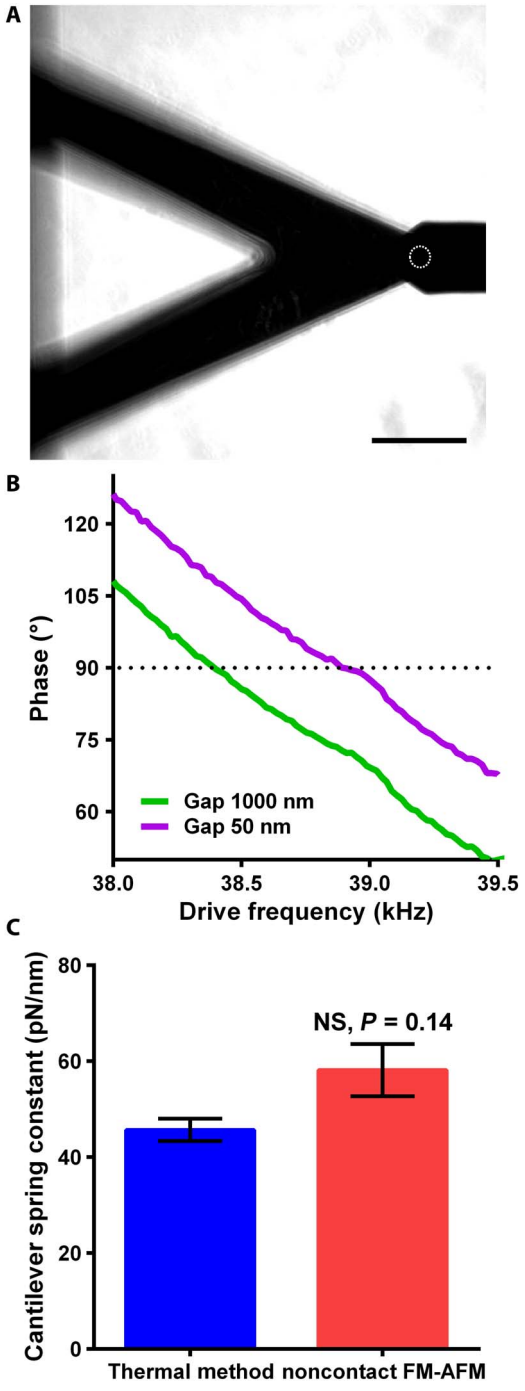

Fig. 2. Methodology validation by determining the spring constant of AFM tipless microcantilevers with known value. (**A**) Phase-contrast image showing the AFM cantilever with a 10-μm sphere (white dashed circle) and a tipless AFM cantilever with known stiffness. Scale bar, 45 μm. (**B**) Phase-frequency curves depicting frequency shifts acquired by keeping a constant π/2 phase (dotted line) when the acoustically vibrating cantilever with microsphere is moved from 1 μm to 50 nm from the tipless cantilever. (**C**) Determined AFM tipless cantilever spring constant using standard thermal fluctuations and novel noncontact FM-AFM methods. Data are presented as means ± SEM; NS indicates nonsignificant differences in comparison with controls, $P = 0.14$ (by unpaired two-tailed Student's t test with Welch's correction); numbers of measurements pooled were five tune curves for the thermal method and eight phase-frequency curves for the noncontact FM-AFM.

between the acoustically oscillating micrometer-sized sphere and the hair bundle critically depends on the sphere radius, sphere-to-hair bundle gap, and cantilever resonance frequency. Specifically, the applied force can be estimated as the product of the hydrodynamic mass ΔM and the acceleration of the sphere $\omega^2 A$, in which A is the oscillation amplitude and ω is the cantilever resonance frequency in radians per second. Therefore, the applied forces $F = 2k_c A\Delta\omega/\omega$ [equation from (*24*)] were about 1 to 10 pN in our experiments, similar to the physiological forces applied during normal hearing (*30*). In contrast, the applied forces by stiff microprobes for bundle stimulation in the excitatory/inhibitory direction are typically 10- to 1000-fold larger (*17*, *18*).

FM-AFM measures the bundle stiffness normal to the hair bundle

The method is sensitive to measure the sensory hair bundle stiffness normal to the hair bundle and with negligible influences from the bundle axial stiffness or the reticular lamina apical surface stiffness. Stereocilia are mechanosensory protrusions filled with crystalline F-actin (*31*). This is consistent with the notion that stereocilia are rigid and difficult to compress or buckle (*32*); thus, it is unlikely that, with a low applied force in the range of 1 to 10 pN, we could measure the bundle axial stiffness. In addition, using the peak force tapping AFM (PFT-AFM) imaging modality, we measured the surface normal stiffness of the apical turn reticular lamina (OHC cuticular plate and supporting cells' apical surface) and observed that the stiffness at P17 is ~5 to 10 times higher than the measured sensory hair bundle stiffness normal to the hair bundle (fig. S1). Therefore, it is unlikely that FM-AFM will measure the reticular lamina apical surface stiffness when the oscillating bead is positioned over a hair bundle. Together, these results show that we mostly measure the hair bundle stiffness normal to the hair bundle.

Estimation of hair bundle geometrical parameters in the $^1/_4$ apical turn of the cochlea

Stereocilia hair bundle effective area and sensory epithelial angle are critical geometrical parameters required for the determination of hair bundle stiffness. We used scanning electron microscopy (SEM) to acquire images of the apical turn hair bundles at different postnatal ages (P10, P12, and P14) and estimated the effective area at the top of the bundle (fig. S2). We observed that the OHC stereocilia bundle in $Strc^{-/-}/Tecta^{-/-}$ mice at P14 had a significantly larger effective area at the top of the bundle compared to $Strc^{+/-}/Tecta^{-/-}$ heterozygous littermates (6.4 ± 0.4 μm^2 versus 5.3 ± 0.2 μm^2; fig. S2). Close examination of SEM images confirmed that horizontal top connectors are absent in OHC bundles from mutant $Strc^{-/-}/Tecta^{-/-}$ mice at P14 and that the space between the apices of individual stereocilia is larger than that in $Strc^{+/-}/Tecta^{-/-}$ bundles (fig. S2). This result confirms the role played by horizontal top connectors in OHC stereociliary bundle cohesiveness. In addition, to determine the sensory epithelium angle, we used confocal fluorescence microscopy (fig. S3) to image P10, P12, and P14 $Tecta^{-/-}$ (single knockout) cochlear cryosections through the apical turn. Assuming that the tallest stereocilia row is orthogonal to the hair cell cuticular plate and reticular lamina, we estimated the reticular lamina angle with respect to the horizontal basilar membrane in the apical turn for P10, P12, and P14 $Tecta^{-/-}$ mice to be 4° ± 0.5°, 6.7° ± 0.9°, and 15.2° ± 0.7°, respectively (fig. S3). We performed a sensitivity analysis to estimate the effects of measured geometrical parameters epithelial angle β and the hair bundle area A_b in bundle stiffness calculations

and obtained ($\Delta\beta/\beta$) ~ 12.5% and ($\Delta A_b/A_b$) ~ 7.7% uncertainty in k_b (section S3). Together, we observed significant differences in hair bundle geometrical parameters measured in the organ of Corti apical turn (effective area at the top of the bundle and sensory epithelium angle) that cannot be ignored when measuring the bundle mechanics.

Absence of horizontal top connectors markedly reduces OHC stereocilia bundle stiffness

We used our method to measure stereocilia bundle stiffness of mature IHCs and OHCs and determine the contribution of horizontal top connectors to OHC hair bundle stiffness. These apical linkers, which are perpendicular to the stereocilia shafts, interconnect neighboring stereocilia (within and between adjacent rows) of the mature bundle. To minimize bundle damage generated by the peeling off of the tectorial membrane in which the tallest stereocilia are embedded from P8 to P9 (*14*), we generated stereocilin and α-tectorin (*Tecta*$^{-/-}$) (*26*) double-knockout mice with a constitutively detached abnormal tectorial membrane. FM-AFM was used to measure the hair bundle stiffness of *Strc*$^{+/-}$/*Tecta*$^{-/-}$ controls and *Strc*$^{-/-}$/*Tecta*$^{-/-}$ mice lacking top connectors, both with detached tectorial membrane. All FM-AFM experiments were performed on explants from the apical $^1/_4$ turn. To verify explant viability and physiological MET channel functionality, we added 500 nM Calcein-AM or 5 μM FM1-43X dye and performed combined confocal and AFM experiments (Fig. 3). Figure 3B and fig. S4 show hair cells with functional MET channels using the FM1-43 vital fluorescence dye at two different incubation times: 20 s and 3 min. It has been shown that during incubation with FM1-43 of the organ of Corti for a short period (on a timescale of seconds to a few minutes), the dye enters the sensory hair cells mostly through their hair bundles and not significantly through endocytosis (*33*). These results show that, during combined confocal and AFM experiments, hair cells are healthy and have functional MET channels.

We first measured the stereocilia bundle passive stiffness of control heterozygous littermate OHCs and IHCs at ages P13 to P15. We recorded frequency sweeps for different ranges around the resonance frequency $f_{\pi/2}$, where the phase was set to π/2 at a distance of 1 μm (Fig. 4, A and B). Since the AFM cantilever with an attached micrometer-sized bead is set to oscillate at 30 to 45 kHz, and these frequencies are much higher than the excitatory hair bundle frequency in the apical turn in mice (~4 to 10 kHz) (*34*), we can assume that we are measuring passive bundle mechanics. The obtained value was 5.12 ± 0.46 pN nm^{-1} for OHCs (Fig. 4C). We found an IHC hair bundle stiffness of 2.34 ± 0.64 pN nm^{-1}, which is ~55% lower compared to the OHCs (Fig. 4D). This is consistent with previous studies in the guinea pig cochlea showing that IHC stereocilia bundles are much softer than OHC ones (*17*).

We then investigated the hair bundle passive mechanics when stereocilin is absent. The frequency shift was significantly larger for *Strc*$^{+/-}$/*Tecta*$^{-/-}$ OHCs than for *Strc*$^{-/-}$/*Tecta*$^{-/-}$ OHCs, indicating a difference in bundle stiffness (Fig. 4, A and B). Using Eq. 1 to calculate the bundle stiffness, we found that the absence of OHC horizontal top connectors in P13 to P15 mice markedly reduces the bundle stiffness by ~60% (2.05 ± 0.15 pN nm^{-1} versus 5.12 ± 0.46 pN nm^{-1}; Fig. 4C), i.e., to levels comparable to IHC bundle stiffness. In these latter cells, bundle stiffness is unaffected by the absence of stereocilin (2.74 ± 0.5 pN nm^{-1} versus 2.34 ± 0.64 pN nm^{-1}; Fig. 4D), as expected by the absence of stereocilin in their hair bundle (*14*). These results indicate that horizontal top connectors are major contributors to OHC hair bundle stiffness.

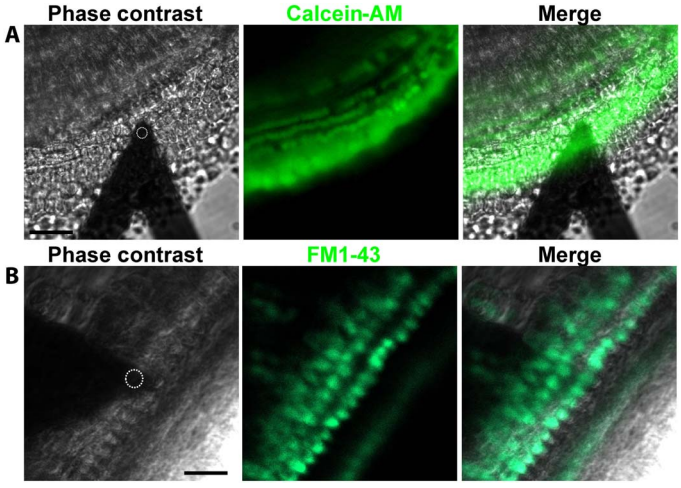

Fig. 3. Visualization of viable cochlear apical turn hair cells during noncontact FM-AFM measurements. (**A** and **B**) Phase-contrast images showing the localization of the AFM cantilever with a 10-μm sphere (white dashed circle) over the OHCs. (A) Representative confocal image of the apical turn cells labeled with Calcein-AM confirming tissue viability. Scale bar, 45 μm. (B) Representative confocal image of the apical turn sensory epithelium transducing OHCs and IHCs labeled with 5 μM FM1-43, confirming hair cells' proper MET channel functionality. Note that, with the 3-min incubation time used, cytoplasmic labeling of the sensory hair cells indicates that FM1-43 enters the cells mostly through their MET channels and not significantly through endocytosis (*33*). Scale bar, 25 μm. Images (A and B) were collected at the apical turn from different *Strc*$^{+/-}$/*Tecta*$^{-/-}$ mice at P14.

Absence of horizontal top connectors reduces OHC stereocilia bundle damping

There is a need to experimentally determine the mechanosensory cell hair bundle viscous damping parameter to help modelers use physiologically relevant values. To do this, we treated the stereocilia bundle as a Kelvin-Voigt viscoelastic element consisting of elastic and viscous components (k_b and c_b). See section S2 for detailed derivation. The bundle damping is determined from

$$c_b = -\frac{3k_b}{A_b \sin\beta}\frac{1}{\pi f_{far}^2 \frac{d\phi}{df}} \quad (2)$$

where c_b (Pa·s m^{-1}) is the global bundle damping parameter, ϕ (rad) is the cantilever response phase, and $\frac{d\phi}{df}$ (rad Hz^{-1}) is the slope of the phase-frequency curve. Measurements of the slope of the phase-frequency curves at different distances from OHC bundles are shown in Fig. 5A. The Phase denotes the phase difference between the piezo and the microsphere oscillation. When the vibrating sphere is moved closer to the hair bundle, changes in $d\phi/df$ measured at $f_{\pi/2}$ are negligible.

We determined the hair bundle viscous damping of control *Strc*$^{+/-}$/*Tecta*$^{-/-}$ and mutant *Strc*$^{-/-}$/*Tecta*$^{-/-}$ OHCs and IHCs from P13 to P15 cochleas. For OHCs, we found damping parameter values of 10.76 ± 1.2 kPa·s m^{-1} and 2.85 ± 0.3 kPa·s m^{-1} in control and stereocilin-deficient mice, respectively (Fig. 5B). The absence of top connectors thus significantly reduces the bundle damping by ~74%. Furthermore, consistent with bundle stiffness results, we found that IHC bundle damping was unaffected in the absence of stereocilin (Fig. 5C). These results indicate that the horizontal top connectors are essential for normal OHC bundle damping.

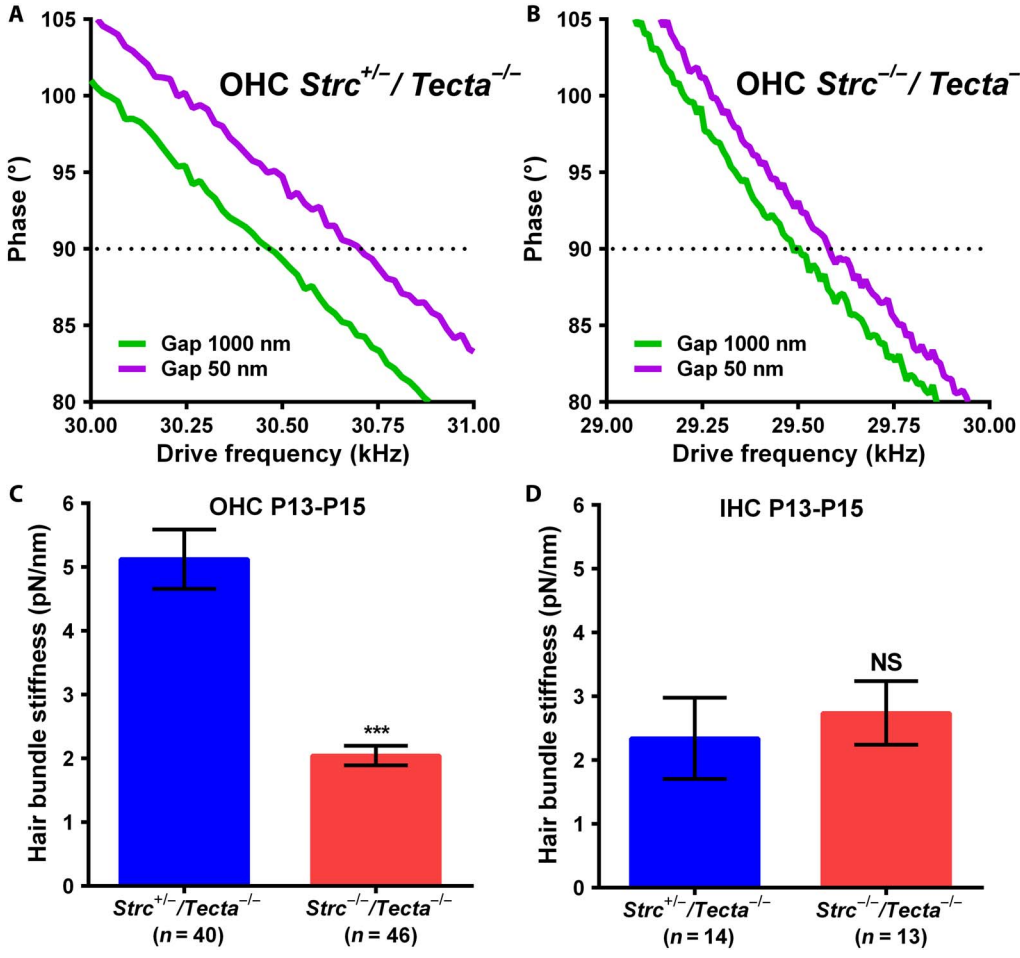

Fig. 4. Deletion of stereocilin markedly reduces the OHC stereociliary bundle stiffness, whereas IHC bundle stiffness is unaffected. (**A** and **B**) Phase-frequency curves obtained for P14 *Strc*$^{+/-}$/*Tecta*$^{-/-}$ (A) or *Strc*$^{-/-}$/*Tecta*$^{-/-}$ (B) OHCs from the apical turn of the cochlea. Acquisitions were done with a constant π/2 phase (dotted line) when the acoustically vibrating cantilever with a 10-μm microsphere was moved from 1 μm to within 50 nm from the top of the tall stereocilia row. (**C** and **D**) In the absence of stereocilin, the OHC hair bundle stiffness is markedly reduced (C), but the IHC bundle stiffness is unaffected (D). Data are presented as means ± SEM; *** indicates significant differences in comparison with heterozygous littermate controls, $P < 0.05$ (by unpaired two-tailed Student's *t* test with Welch's correction); NS indicates nonsignificant differences in comparison with controls, $P > 0.05$ (by unpaired two-tailed Student's *t* test with Welch's correction); the indicated number of cells used was from seven animals for *Strc*$^{+/-}$/*Tecta*$^{-/-}$ ($n = 40$) and seven animals for *Strc*$^{-/-}$/*Tecta*$^{-/-}$ ($n = 46$) OHCs and from five animals for *Strc*$^{+/-}$/*Tecta*$^{-/-}$ ($n = 14$) and four animals for *Strc*$^{-/-}$/*Tecta*$^{-/-}$ ($n = 13$) IHCs.

Apical turn OHC bundle stiffness and damping significantly increase during development of horizontal top connectors

Developmental changes in stereocilia bundle stiffness provide critical insight into the maturation process of the hair bundle and could help identify the most structurally important molecular components during late developmental stages around the onset of hearing at about P12. In the developing OHCs, stereocilin is first detected at P2 around the kinocilium (a genuine transient cilium) and from P3 at the apex of the tallest stereocilia row where the tectorial membrane attachment crowns are developing. Between P10 and P12 in the apical part of the cochlea, stereocilin progressively appears in the middle and then in the shortest row of stereocilia, concomitant with the formation of horizontal top connectors (*11*). Several structural changes occur during the postnatal development of the mechanosensory hair bundle, including the growth (in length and width) of stereocilia (*35*), the disappearance of transient lateral and ankle links concomitantly with the appearance of horizontal top connectors (*11*), and the development of stereocilia rootlets (*20*). One might anticipate that these different developmental structural changes in the hair bundle contribute to changes in bundle mechanical properties.

To confirm this hypothesis, we measured the hair bundle mechanics from P9 to P15 in *Strc*$^{+/-}$/*Tecta*$^{-/-}$ and *Strc*$^{-/-}$/*Tecta*$^{-/-}$ OHCs using tissue explanted from the $^{1}/_{4}$ apical turn of the organ of Corti (Fig. 6). We found that the bundle stiffness markedly increases ~6 times (P9 $k_b = 0.92 \pm 0.18$ pN nm^{-1} against P15 $k_b = 5.4 \pm 0.9$ pN nm^{-1}) when horizontal top connectors develop in *Strc*$^{+/-}$/*Tecta*$^{-/-}$ OHCs, while a smaller increase (~2 times) in stiffness (P9 $k_b = 1 \pm 0.16$ pN nm^{-1} against P15 $k_b = 2 \pm 0.2$ pN nm^{-1}) was observed when these links fail to develop in *Strc*$^{-/-}$/*Tecta*$^{-/-}$ OHCs (Fig. 6A). Furthermore, in line with the bundle stiffness trend, we found that the bundle viscous damping significantly increases with the development of top connectors in *Strc*$^{+/-}$/*Tecta*$^{-/-}$ OHCs (P9 $c_b = 2.8 \pm 1$ kPa·s m^{-1} against P15 $c_b = 15.3 \pm 4.3$ kPa·s m^{-1}). Unexpectedly, damping in *Strc*$^{-/-}$/*Tecta*$^{-/-}$ OHCs appeared constant and did not show significant changes between P9 and P15 (P9 $c_b = 4.1 \pm 0.7$ kPa·s m^{-1} against P15 $c_b = 3 \pm 0.5$ kPa·s m^{-1}) (Fig. 6B). The OHC bundle stiffness increase between P9 and P15 in

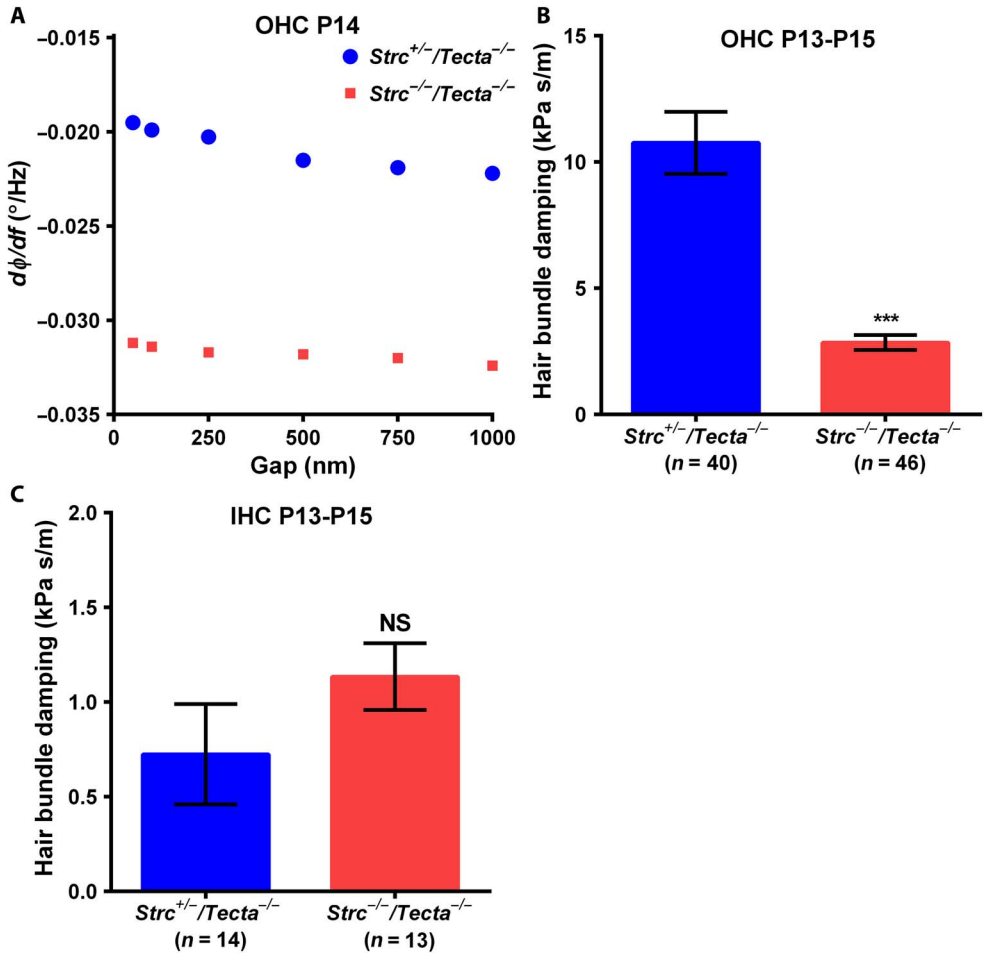

Fig. 5. OHC and IHC hair bundle viscous damping parameter. (**A**) Changes in the slope of the phase-frequency curve acquired on an apical turn OHC stereocilia bundle from P14 $Strc^{+/-}/Tecta^{-/-}$ (blue circles) and $Strc^{-/-}/Tecta^{-/-}$ (red squares) mice. When the acoustically oscillating 10-μm sphere is moved closer to the sensory hair bundles, changes in $d\Phi/df$ measured at $f_{\pi/2}$ are negligible. (**B** and **C**) In the absence of stereocilin, the damping parameter is significantly reduced in OHCs (B) but unaffected in IHCs (C). Note that cochlear IHC bundles have elevated fluid-like behavior compared to OHCs, since their hydrodynamic frictional drag is reduced compared to OHCs. Data are presented as means ± SEM; *** indicates significant differences in comparison with heterozygous littermate controls, $P < 0.05$ (by unpaired two-tailed Student's *t* test with Welch's correction); NS indicates nonsignificant differences in comparison with controls, $P > 0.05$ (by unpaired two-tailed Student's *t* test with Welch's correction); the indicated number of cells used was from seven animals for $Strc^{+/-}/Tecta^{-/-}$ ($n = 40$) and seven animals for $Strc^{-/-}/Tecta^{-/-}$ ($n = 46$) OHCs and from five animals for $Strc^{+/-}/Tecta^{-/-}$ ($n = 14$) and four animals for $Strc^{-/-}/Tecta^{-/-}$ ($n = 13$) IHCs.

the absence of stereocilin could be explained by the formation and thickening of individual stereocilia rootlets and the increase in stereocilia width, since an increase in stereocilia height and loss of transient lateral links and ankle links are rather expected to decrease the hair bundle stiffness and viscous damping. Our results also suggest that TM attachment crowns, which are well developed in $Tecta^{-/-}$ mice (*14*), do not contribute significantly to the hair bundle stiffness and damping. We observed no significant difference in bundle stiffness and damping between $Strc^{+/-}/Tecta^{-/-}$ and $Strc^{-/-}/Tecta^{-/-}$ OHCs at ages P9 to P11, i.e., when the tectorial membrane attachment crowns are already present in $Strc^{+/-}/Tecta^{-/-}$ mice. Together, these results highlight the critical contribution of horizontal top connectors to hair bundle mechanics during postnatal development.

DISCUSSION

Here, we presented a noncontact FM-AFM method capable of determining hair bundle mechanics. Our method is more physiologically relevant than conventional contact methods because it does not require any labeling of the tissue or any physical contact with the stimulating microbead. The stereocilia bundle is stimulated at acoustic frequencies, and the applied forces are in the physiological range of 1 to 10 pN. Recently published studies showed that conventional stiff microprobes stimulate the hair bundle unevenly in the excitatory direction and also apply large forces potentially causing splaying of hair bundles, thus leading to underestimation of the overall bundle stiffness (*36*, *37*). In addition, because of the large bundle deflection induced by stiff microprobes, it is likely that irreversible bundle damage can occur from breakage of interstereocilia links. Our method, using a high-frequency oscillating microsphere with nanoscale gaps above the tallest stereocilia row, generates a hydrodynamic interaction force that causes a cyclical orbital stimulation similar to sound-induced stimulation of the hair cell bundles (*27*, *38*). We also developed simple-to-use mathematical formulas to relate cantilever frequency shifts to the hair bundle stiffness and damping and thereafter used these formulae to determine the hair bundle stiffness and damping of OHCs and IHCs in mice with a

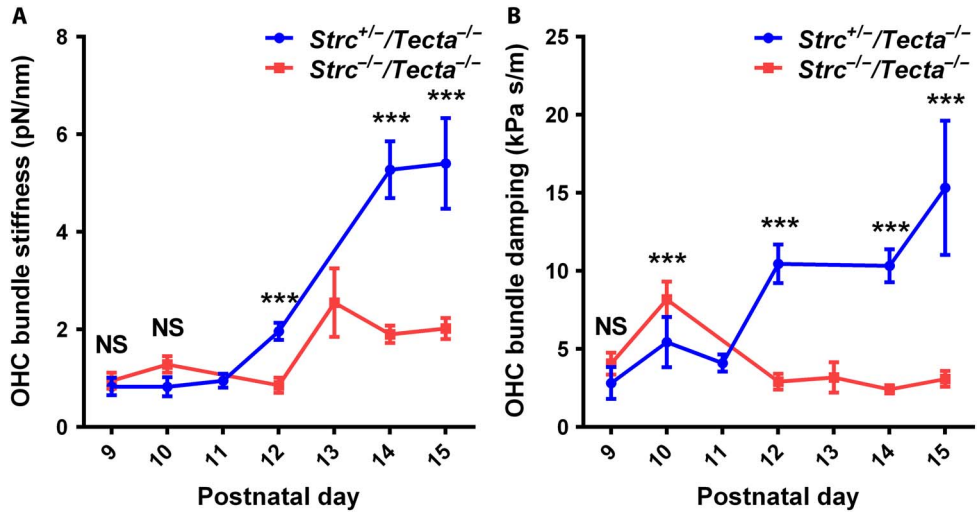

Fig. 6. Developmental changes in apical turn OHC stereociliary bundle stiffness and damping from P9 to P15. Apical turn OHC bundle stiffness (**A**) and bundle damping (**B**) in control $Strc^{+/-}/Tecta^{-/-}$ mice and $Strc^{-/-}/Tecta^{-/-}$ mice lacking horizontal top connectors. At P9 and P10, the bundle stiffness values show no significant differences, whereas the viscous damping shows significant difference at P10. From P12 onward, bundle stiffness and damping markedly increase in $Strc^{+/-}/Tecta^{-/-}$ OHCs. Data are presented as means ± SEM; *** indicates significant differences, $P < 0.05$ (by unpaired two-tailed Student's *t* test with Welch's correction); NS indicates nonsignificant differences, $P > 0.05$ (by unpaired two-tailed Student's *t* test with Welch's correction); number of measurements pooled per postnatal day (animals, cells) for $Strc^{+/-}/Tecta^{-/-}$ OHCs [P9 (2, 4), P10 (1, 4), P11 (1, 8), P12 (1, 8), P14 (4, 32), and P15 (2, 8)] and $Strc^{-/-}/Tecta^{-/-}$ OHCs [P9 (1, 11), P10 (2, 16), P12 (1, 6), P13 (1, 6), P14 (3, 17), and P15 (3, 23)].

constitutively detached tectorial membrane. Using these animals allowed us to minimize hair bundle damage that is commonly caused by tectorial membrane peeling off from the explant and may lead to underestimation of the stiffness and damping at mature postnatal ages. Therefore, noncontact FM-AFM combined with a genetically modified mouse with detached tectorial membrane should be of broad application for deciphering the molecular regulation of sensory hair bundle mechanics.

The mouse apical turn OHC bundle stiffness measured shortly after the onset of hearing (postnatal ages P13 to P15) is significantly larger than those measured at early mouse postnatal ages or in rats. To our knowledge, the only measurement of OHC bundle stiffness in the mouse has been done in early P1 to P5 cochlear cultures (*23*). The apical turn OHC stereocilia bundle stiffness values measured by our noncontact FM-AFM method is ~5.12 ± 0.46 pN nm^{-1} at P13 to P15, which are ~2 to 5 times larger than the ones obtained using stiff microprobes in wild-type mice at early postnatal ages P1 to P5 (*23*). The larger stiffness value obtained by FM-AFM could be explained in part by the fact that, at early postnatal stages P1 to P5, the sensory hair cell bundles are not fully developed. The stereocilia bundles, which continue to elongate at early P1 to P5 ages, are interconnected with a dense web of transient links all along their shaft. The stiffness of more mature OHC bundle has been measured in the rat at P7 to P11 (*18*). The obtained values of 1 to 3 pN nm^{-1} are 1.5 to 5 times lower than the values obtained herein at P13 to P15 in the mouse. The following are possible explanations for this discrepancy: (i) Top connectors are not fully mature in the rat at P7 to P11, (ii) stiffness may be different in the two species at comparable stages of development, (iii) the type of bundle stimulation is different, and (iv) the bundles are damaged by the removal of the tectorial membrane in the rat. Together, these results indicate that we should be cautious when comparing sensory hair OHC bundle mechanical properties measured at different stages of development, in different species, and/or with different methods.

Our noncontact FM-AFM is also capable of determining the sensory hair bundle viscous damping. The viscous damping calculated for normal OHC bundles was significantly larger than that for bundles without horizontal top connectors. This result suggests that bundle coherence is strongly dependent on both elastic stiffness and viscous damping, because sensory hair bundles are intrinsically damped structures. The coupling of bundle stiffness and damping parameters could depend on stereocilin itself or on other stereocilin binding partners needed to form the horizontal top connectors. The recently reported viscous hydrodynamic friction coefficient of the hair bundle in a bullfrog's sacculus (sensory area of the balance organ) (*39*, *40*) and our measured effective bundle viscosity are of the same order of magnitude, providing confidence that our described noncontact method is capable of measuring the hair bundle mechanics with high accuracy. Nevertheless, to the best of our knowledge, this is the first time the viscous damping parameter of the mice cochlear hair bundles has been determined experimentally using acoustic frequency stimulations.

Previous studies on stereocilin-deficient mice have shown that horizontal top connectors maintain adjacent stereocilia in close apposition and allow a synchronous motion of all stereocilia of one OHC bundle (*13*, *14*). Here, we show that horizontal top connectors are also major contributors to stiffness and damping of the mature OHC hair bundle. As stereocilin is an extracellular protein (*14*), which cannot affect the organization of the crystalline F-actin, its absence is not expected to affect the rigidity of each individual stereocilium. The observed decrease in passive bundle stiffness by 60% in stereocilin-deficient mice lacking horizontal top connectors is thus more than likely due to the partial loss of cohesiveness of the OHC hair bundle in which adjacent stereocilia are interconnected only between rows by the tip links and with no connections within a row.

By following the bundle mechanics of $Strc^{+/-}/Tecta^{-/-}$ and $Strc^{-/-}/Tecta^{-/-}$ OHCs between P9 and P15, we confirmed that the top connectors are the major contributors to OHC hair bundle mechanics. During postnatal development of the OHC hair bundle, developmental features such as growth of stereocilia, disappearance of transient links, and development of stereocilia rootlets are not expected to be different in the two groups of mice whose OHC hair

bundles differ only by the presence of the tectorial membrane attachment crowns and the horizontal top connectors. As no difference in stiffness or damping values was observed before P12, the tectorial membrane attachment crowns, which develop from P2 in *Strc*$^{+/-}$/*Tecta*$^{-/-}$ mice, do not contribute significantly to OHC hair bundle mechanics. On the other hand, we found that the hair bundle stiffness increased in both *Strc*$^{+/-}$/*Tecta*$^{-/-}$ and *Strc*$^{-/-}$/*Tecta*$^{-/-}$ mice from P12, but the increase was much higher in *Strc*$^{+/-}$/*Tecta*$^{-/-}$ than in *Strc*$^{-/-}$/*Tecta*$^{-/-}$ mice (~6- and ~2-fold, respectively). Hair bundle damping also increased, only in *Strc*$^{+/-}$/*Tecta*$^{-/-}$ mice, from P12, i.e., when horizontal top connectors develop and mature in the apical part of the cochlea.

Findings obtained in the bullfrog sacculus have shown, by combining modeling and imaging, that tip links alone are unable to explain the observed bundle coherent motion as a single unit (*6*), indicating that tip links are not dominant contributors to bundle rotational stiffness, to the passive micromechanical architecture of the hair bundle, and to the dynamic coherent bundle motion. In line with this result, Karavitaki and Corey (*5*) showed that, in the bullfrog saccular hair cells, absence of horizontal top connectors results in larger deflections of bundles not observed when tip links, ankle links, or shaft connectors are removed. Horizontal top connectors of the bullfrog saccular hair cells are very different from mammalian OHCs in structure. However, in both hair cell types, these apical horizontal links between adjacent stereocilia seem to be major contributors to hair bundle stiffness and damping, the maintenance of the highly cohesive architecture of the bundle, and the mechanical coupling of the MET channels.

In summary, this study demonstrates the usefulness of noncontact FM-AFM with stimulations relevant to hearing to measure the stiffness and viscous damping of mature OHCs. Our data reveal that horizontal top connectors are major contributors to the mature OHC hair bundle micromechanical architecture necessary for the maintenance of the OHC bundle functionality.

MATERIALS AND METHODS

Generation of stereocilin and α-tectorin double-knockout mice

Stereocilin (*Strc*$^{tm1Ugds/tm1Ugds}$, referred to as *Strc*$^{-/-}$) and α-tectorin (*Tecta*$^{\Delta ENT/\Delta ENT}$, referred to as *Tecta*$^{-/-}$) mice were described in previous studies (*12*–*14*, *26*). *Tecta*$^{\Delta ENT/\Delta ENT}$ mice were provided by G. Richardson (University of Sussex, Falmer, UK). The targeted deletion of exons 2 and 3 in *Strc*$^{-/-}$ mice results in a frameshifting deletion that would produce an incomplete signal peptide followed by 30 out-of-frame amino acids (*13*). Targeted integration of a *neo*^{r} cassette into exon 4 of *Tecta* results in the skipping of this exon, which is predicted to cause a deletion of 96 amino acids in α-tectorin. The protein is not detected by Western blot analysis in *Tecta*$^{\Delta ENT/\Delta ENT}$ cochleae (*26*). *Strc*$^{-/-}$/*Tecta*$^{-/-}$ double-knockout mice were produced by breeding *Strc*$^{-/-}$ mice with *Tecta*$^{-/-}$ mice and the compound heterozygous offspring with each other. *Strc*$^{-/-}$/*Tecta*$^{-/-}$ mice were mated to *Strc*$^{+/-}$/*Tecta*$^{-/-}$ mice to generate *Strc*$^{-/-}$/*Tecta*$^{-/-}$ and *Strc*$^{+/-}$/*Tecta*$^{-/-}$ littermate controls.

Strc genotyping of experimental animals was performed using two separate polymerase chain reactions (PCRs) with forward primers F_1 (5′-GGGCTCTGAGGAGGCTCTTTGGG-3′) [located in exon 2 (reaction 1)] and F_2 (5′-TGGGATTTGAACTCAGGTTGCTAGG-3′) [located in intron 1 (reaction 2)], respectively, and reverse primer R_2 (5′-CAGAGGCACACCTCTGCTCAGG-3′) (located in exon 4) (*13*). Because of the targeted deletion of exons 2 and 3, there is no amplification product for the *Strc*$^{-}$ allele in reaction 1, and reaction 2 gives an amplicon size of 1 kb. The size of the products amplified from the wild-type allele is 1250 base pairs (bp; reaction 1) and 2300 bp (reaction 2) (fig. S5, A and B). *Tecta* genotyping was performed using forward primer 5′-TTACAGGCGTGGTACTGCTG in exon 4 and reverse primer 5′-TGGTGTTGTTTCCTTCAACG spanning the exon 4–intron 4 boundary. Experimental mice (*Strc*$^{+/-}$ or *Strc*$^{-/-}$) are all homozygous for the *Tecta*$^{-}$ allele and thus give a single 2.1-kb amplicon, owing to the insertion of the *neo*^{r} cassette into exon 4. Amplification from a wild-type allele would give a 281-bp fragment (fig. S5, C and D).

Organ of Corti explant preparation

Cochleas from *Strc*$^{+/-}$/*Tecta*$^{-/-}$ and *Strc*$^{-/-}$/*Tecta*$^{-/-}$ mice pups of postnatal ages P9 to P15 were dissected to expose the sensory epithelium and plated on precoated glass-bottom petri dishes (WillCo Wells BV, Amsterdam, Netherlands) in fresh Leibovitz's medium (Life Technologies, Carlsbad, CA). The glass dishes were precoated with 100 μl of Matrigel mixture [250 μl of Matrigel (Corning Life Sciences, Corning, NY) diluted in 5 ml of Hanks' balanced salt solution (HBSS)] or with 10 μl of Cell-Tak (Corning) spread on the glass, placed inside an incubator at 37°C for 30 min, and rinsed twice with fresh phosphate-buffered saline (PBS) to form a thin-layer coating. For the viability assessment experiment, the explants were incubated in 500 nM Calcein-AM vital dye (Life Technologies) in Leibovitz's culture medium for 30 min in a tissue culture incubator at 37°C and 5% CO_2 and then rinsed with fresh Leibovitz medium. To ensure that our procedures used to prepare the explants for FM-AFM preserved the tip links, we performed MET channel functionality tests on some explants. FM1-43X dye (5 μM; Life Technologies) was added for 20 s or 3 min inside an incubator at 37°C, rapidly washed twice with fresh Leibovitz media, and then immediately viewed (within 2 min) using a confocal Laser Scanning Microscope 510 Meta (LSM 510 Meta, Carl Zeiss). The cochlear explants were placed inside an incubator for 30 min before FM-AFM experiments. For all experiments, male and female mice were used randomly. Note that some sensory hair bundle mechanical property measurements were performed on cochlear explants with FM1-43 staining to identify bundles that are functional. However, since almost all hair cells incorporated staining by 20 s and the determined bundle stiffness and damping were similar to unstained explants, we performed most of the FM-AFM experiments on unstained explants.

Noncontact frequency-modulated AFM

FM-AFM experiments were performed using a Bruker Bioscope Catalyst AFM system (Bruker Inc., Santa Barbara, CA, USA) mounted on an inverted Axiovert 200M microscope system (Carl Zeiss, Göttingen, Germany) equipped with a confocal LSM 510 Meta (Carl Zeiss) and a 40× (0.6 numerical aperture; Plan-Apochromat) objective lens (Carl Zeiss). The AFM biological system was placed on a vibration isolation table (Kinetic Systems, Boston, MA, USA). A heating stage (Bruker) was used to maintain the physiological temperature (37°C) of explants during measurements. Modified triangular, gold-coated, silicon nitride AFM cantilevers with a 10-μm borosilicate glass attached microsphere were obtained from Novascan (Novascan, Ames, IA, USA). The cantilevers were precalibrated by the company before microsphere attachment with a calibrated spring constant of ~0.12 N m^{-1}. We confirmed calibrations by using the thermal fluctuation tune method (*29*) built in the AFM system. AFM microcantilevers' calibrated spring constants were 0.1 to 0.17 N m^{-1}.

Once the cochlear explant was placed in the AFM X-Y sample stage, the cantilever was positioned in liquid far above the sample

surface and allowed to thermally equilibrate. For noncontact acoustic FM-AFM experiments, tapping mode AFM was engaged. Immediately, the cantilever tune mode was launched to choose the driving frequency. An initial frequency sweep was performed to locate $f_{\pi/2}$. Because we used piezo-driven excitation in liquids, a forest of peaks is observed (*41*). We chose the largest peak found with a well-defined phase change, with a typical resonant frequency of 30 to 45 kHz. Next, the cantilever was approached and gently placed in contact with the hair cell bundle. Then, the cantilever tune mode was launched and initially set to position the microsphere of the cantilever 1 μm above the hair bundle, and the phase lag between the piezo and the cantilever was set to π/2. In addition, the drive oscillatory amplitude of the piezo was adjusted to ensure that the cantilever oscillation amplitude at $f_{\pi/2}$ was 5 nm or below. Frequency sweeps were recorded with a 10-kHz frequency range around $f_{\pi/2}$ for multiple distances between the bead and the hair bundle from 1 μm or 500 nm down to 50 nm. Last, the vibrating cantilever was moved 4 μm away for the surface, and a final frequency sweep was recorded to acquire f_{∞}. Note that this methodology derives from (*25*).

FM-AFM data analysis

All computations were performed using the software MATLAB (MathWorks, Natick, MA, USA). The phase-frequency curves recorded at different distances from the sample surface were extracted as ASCII files using Bruker's Nanoscope Analysis software and loaded into MATLAB. The curves were fitted with a second-order polynomial on the vicinity of π/2 to determine the frequency $f_{\pi/2}$ at different gaps. Then, the frequency shift $\Delta f_{\pi/2}$ in the bead oscillation was determined by the difference between the acquired frequencies where the phase lag is kept constant at π/2 of the unperturbed sphere placed far from the hair bundle (1 μm) and the perturbed sphere when placed within 50 nm from the top of the tall stereocilia row: $\Delta f_{\pi/2} = f_{\text{near},\pi/2} - f_{\text{far},\pi/2}$. In addition, the phase-frequency curves' slope $d\phi/df$ was computed using the frequency sweeps recorded at 50 nm above the hair bundle by fitting the phase-frequency curves with a third-order polynomial. Estimates of $d\phi/df$ did not change significantly between the measured height range over the sensory cell hair bundle (Fig. 5A).

Peak force tapping AFM

PFT-AFM experiments were performed on P17 organ of Corti explants from $Strc^{+/-}/Tecta^{-/-}$ mice. The AFM probe used was specially designed for PFT-AFM live-cell imaging (PFQNM-LC probe; Bruker) and had a tip height of 17 μm, a controlled tip radius of 65 nm, and an opening half-angle of 15°. The cantilevers were precalibrated by the company using a laser Doppler vibrometer, and the spring constant range of the cantilever used in this study was 0.07 to 0.09 N m^{-1}. We used a peak force driving frequency of 500 Hz and driving amplitudes of 550 to 650 nm. The nominal line scan rate used was 0.4 Hz. The peak force feedback was set between 800 pN and 1.5 nN. The scan resolution of all recorded images was 256 × 256 pixels.

Scanning electron microscopy

For each age (P10, P12, and P14), samples from $Strc^{+/-}/Tecta^{-/-}$ and $Strc^{-/-}/Tecta^{-/-}$ littermates were prepared in parallel. Inner ears were fixed overnight at 4°C in 2.5% glutaraldehyde in 0.1 M sodium cacodylate buffer. After five rapid washes in the cacodylate buffer, the organ of Corti was microdissected and processed according to the osmium tetroxide/thiocarbohydrazide method, as previously described (*42*). After dehydration in graded ethanol solutions and critical point drying with liquid CO_2, samples were mounted on aluminum stubs with carbon tab adhesive (Agar Scientific, Essex, UK). Specimens were imaged in a JEOL JSM-6700F scanning electron microscope (JEOL, Tokyo, Japan) operating at 3 to 5 kV.

SEM image analysis

SEM images from the $^1/_4$ apical turn of the cochlea of P10, P12, and P14 $Strc^{+/-}/Tecta^{-/-}$ and $Strc^{-/-}/Tecta^{-/-}$ mice were analyzed using ImageJ software [National Institutes of Health (NIH), Bethesda, MD, USA] to measure the stereocilia hair bundle effective area at the top of the bundle (A_b). We used the selection brush tool to generate a yellow contour (fig. S2) around stereociliary bundles and determined the area under the contour. Last, we defined three separate groups: P9 and P10 mice with an effective area equal to measurements at P10, intermediate P11 and P12 mice with an effective area equal to measurements at P12, and P13 to P15 mice with an effective area equal to measurements at P14. The reasoning behind the generation of groups was the development of horizontal top connectors. Around P11 is when stereocilin appears in the cochlea apical coil turn and progressively matures (*14*). Therefore, we believe that it is adequate to assume that, from P13 to P15, the effective areas are equal because of the presence of horizontal top connectors.

Confocal fluorescence microscopy on inner ear cryosections

Inner ears were fixed in 4% paraformaldehyde (PFA) in PBS (pH 7.4) for 1 hour at room temperature. After three PBS washes (10 min each), inner ears were decalcified in 0.35 M EDTA in PBS (pH 7.5) at 4°C for 24 hours. After three additional PBS washes, samples were fixed again in 4% PFA in PBS (pH 7.4) for 1 hour at room temperature, washed again in PBS, and then immersed in 30% sucrose in PBS for at least 12 hours at 4°C. They were then transferred in Tissue-Tek embedding medium (Sakura Finetek, Torrance, CA, USA) and frozen. Cryosections (12 μm thick) were collected on Superfrost Plus microscope slides (Thermo Fisher Scientific) and stored at −20°C until use. After rehydration (30 min in PBS), sections were incubated for 1 hour at room temperature in PBS containing 1% bovine serum albumin (BSA) and 0.2% Triton X-100 before staining for 3 hours at room temperature with ATTO 488–conjugated wheat germ agglutinin (50 μg ml^{-1}; Thermo Fisher Scientific) and ATTO 565–conjugated phalloidin (0.2 μM, Sigma-Aldrich) diluted in 1% BSA in PBS. After two PBS washes, sections were incubated in 1.3 μg ml^{-1} 4′,6-diamidino-2-phenylindole (Sigma-Aldrich) for 10 min at room temperature, and after two additional washes, slides were mounted in FluorSave Reagent (Calbiochem, San Diego, CA, USA). Images of the most apical section of the cochlea were acquired with an LSM 700 Meta confocal microscope (Carl Zeiss).

Immunofluorescence images analysis

Maximum intensity Z-projection confocal images from the most apical sections of P10, P12, and P14 $Strc^{+/+}/Tecta^{-/-}$ cochlea were analyzed using ImageJ software (NIH) to measure the sensory epithelium angle (β) between the reticular lamina and the basilar membrane. We drew two intersecting lines, one parallel to the basilar membrane and another parallel to the reticular lamina. The angle formed between the two intersecting lines was then measured. Last, we defined three separate groups: P9 and P10 mice with an epithelial angle equal to measurements at P10, intermediate P11 and P12 mice with an epithelial angle equal to measurements at P12, and P13 to P15 mice with an epithelial angle equal to measurements at P14. This is to be consistent with our effective

area at the top of the hair bundle group generation assumption. Note that, since stereocilin is only present in the maturing OHC sensory bundles, lack of stereocilin is not expected to affect the architecture of the organ of Corti and thus the sensory epithelium angle. In contrast, as the forming tectorial membrane covers the surface of the sensory epithelium from the 18th or 19th gestational day (*43*), we could not exclude the possibility that the sensory epithelium angle could be different between $Tecta^{+/+}$ and $Tecta^{-/-}$ mice. For this reason, the sensory epithelium angle was measured in $Tecta^{-/-}$ single-knockout mice.

Statistical analysis

Statistical analyses and data plotting were performed using GraphPad Prism 6 software (GraphPad Software). Data statistical analysis for two case groups was performed with an unpaired two-tailed Student's *t* test with Welch's correction. All data presented in the text and figures are represented as means ± SEM. In the figures, significance levels for differences between groups are indicated as $^{***}P < 0.05$.

Code availability

A computer code implemented in MATLAB was used for the analysis of acquired noncontact FM-AFM data to extract the sensory cells' hair bundle stiffness and damping. The computer code is available from the corresponding author upon reasonable request.

SUPPLEMENTARY MATERIALS

Supplementary material for this article is available at http://advances.sciencemag.org/cgi/content/full/5/2/eaat9934/DC1

Section S1. Calculation of stereocilia bundle mechanics

Section S2. Viscoelastic hair bundle—Viscous damping parameter

Section S3. Sensitivity analysis of variations in epithelial angle β and hair bundle area A_b affecting bundle stiffness measurements

Fig. S1. Apical turn reticular lamina surface stiffness.

Fig. S2. Estimation of the effective area at the top of the OHC and IHC stereociliary hair bundles in the apical part of the cochlea.

Fig. S3. Estimation of the sensory epithelium angle in the cochlear apical turn.

Fig. S4. FM1-43 labels almost all apical turn sensory hair cells in 20 s.

Fig. S5. PCR genotyping of experimental mice.

REFERENCES AND NOTES

1. A. J. Hudspeth, Integrating the active process of hair cells with cochlear function. *Nat. Rev. Neurosci.* **15**, 600–614 (2014).
2. P. Dallos, The active cochlea. *J. Neurosci.* **12**, 4575–4585 (1992).
3. W. E. Brownell, C. R. Bader, D. Bertrand, Y. de Ribaupierre, Evoked mechanical responses of isolated cochlear outer hair cells. *Science* **227**, 194–196 (1985).
4. M. C. Liberman, J. Gao, D. Z. Z. He, X. Wu, S. Jia, J. Zuo, Prestin is required for electromotility of the outer hair cell and for the cochlear amplifier. *Nature* **419**, 300–304 (2002).
5. K. D. Karavitaki, D. P. Corey, Sliding adhesion confers coherent motion to hair cell stereocilia and parallel gating to transduction channels. *J. Neurosci.* **30**, 9051–9063 (2010).
6. A. S. Kozlov, T. Risler, A. J. Hudspeth, Coherent motion of stereocilia assures the concerted gating of hair-cell transduction channels. *Nat. Neurosci.* **10**, 87–92 (2007).
7. P. Kazmierczak, H. Sakaguchi, J. Tokita, E. M. Wilson-Kubalek, R. A. Milligan, U. Müller, B. Kachar, Cadherin 23 and protocadherin 15 interact to form tip-link filaments in sensory hair cells. *Nature* **449**, 87–91 (2007).
8. V. Michel, R. J. Goodyear, D. Weil, W. Marcotti, I. Perfettini, U. Wolfrum, C. J. Kros, G. P. Richardson, C. Petit, Cadherin 23 is a component of the transient lateral links in the developing hair bundles of cochlear sensory cells. *Dev. Biol.* **280**, 281–294 (2005).
9. N. Michalski, V. Michel, A. Bahloul, G. Lefèvre, J. Barral, H. Yagi, S. Chardenoux, D. Weil, P. Martin, J.-P. Hardelin, M. Sato, C. Petit, Molecular characterization of the ankle-link complex in cochlear hair cells and its role in the hair bundle functioning. *J. Neurosci.* **27**, 6478–6488 (2007).
10. G. P. Richardson, J. B. de Monvel, C. Petit, How the genetics of deafness illuminates auditory physiology. *Annu. Rev. Physiol.* **73**, 311–334 (2011).
11. R. J. Goodyear, W. Marcotti, C. J. Kros, G. P. Richardson, Development and properties of stereociliary link types in hair cells of the mouse cochlea. *J. Comp. Neurol.* **485**, 75–85 (2005).
12. E. Verpy, S. Masmoudi, I. Zwaenepoel, M. Leibovici, T. P. Hutchin, I. Del Castillo, S. Nouaille, S. Blanchard, S. Lainé, J.-L. Popot, F. Moreno, R. F. Mueller, C. Petit, Mutations in a new gene encoding a protein of the hair bundle cause non-syndromic deafness at the DFNB16 locus. *Nat. Genet.* **29**, 345–349 (2001).
13. E. Verpy, D. Weil, M. Leibovici, R. J. Goodyear, G. Hamard, C. Houdon, G. M. Lefèvre, J.-P. Hardelin, G. P. Richardson, P. Avan, C. Petit, Stereocilin-deficient mice reveal the origin of cochlear waveform distortions. *Nature* **456**, 255–258 (2008).
14. E. Verpy, M. Leibovici, N. Michalski, R. J. Goodyear, C. Houdon, D. Weil, G. P. Richardson, C. Petit, Stereocilin connects outer-hair-cell stereocilia to one another and to the tectorial membrane. *J. Comp. Neurol.* **519**, 194–210 (2011).
15. P. Avan, B. Büki, C. Petit, Auditory distortions: Origins and functions. *Physiol. Rev.* **93**, 1563–1619 (2013).
16. J.-H. Nam, R. Fettiplace, Theoretical conditions for high-frequency hair bundle oscillations in auditory hair cells. *Biophys. J.* **95**, 4948–4962 (2008).
17. D. Strelioff, Å. Flock, Stiffness of sensory-cell hair bundles in the isolated guinea pig cochlea. *Hear. Res.* **15**, 19–28 (1984).
18. H. J. Kennedy, A. C. Crawford, R. Fettiplace, Force generation by mammalian hair bundles supports a role in cochlear amplification. *Nature* **433**, 880–883 (2005).
19. C. J. Kros, A. Rusch, G. P. Richardson, Mechano-electrical transducer currents in hair cells of the cultured neonatal mouse cochlea. *Proc. R. Soc. Lond. Ser. B Biol. Sci.* **249**, 185–193 (1992).
20. S.-I. Kitajiri, T. Sakamoto, I. A. Belyantseva, R. J. Goodyear, R. Stepanyan, I. Fujiwara, J. E. Bird, S. Riazuddin, S. Riazuddin, Z. M. Ahmed, J. E. Hinshaw, J. Sellers, J. R. Bartles, J. A. Hammer III, G. P. Richardson, A. J. Griffith, G. I. Frolenkov, T. B. Friedman, Actin-bundling protein TRIOBP forms resilient rootlets of hair cell stereocilia essential for hearing. *Cell* **141**, 786–798 (2010).
21. A. S. Kozlov, J. Baumgart, T. Risler, C. P. C. Versteegh, A. J. Hudspeth, Forces between clustered stereocilia minimize friction in the ear on a subnanometre scale. *Nature* **474**, 376–379 (2011).
22. A. S. Kozlov, D. Andor-Ardó, A. J. Hudspeth, Anomalous Brownian motion discloses viscoelasticity in the ear's mechanoelectrical-transduction apparatus. *Proc. Natl. Acad. Sci. U.S.A.* **109**, 2896–2901 (2012).
23. I. J. Russell, M. Kössl, G. P. Richardson, Nonlinear mechanical responses of mouse cochlear hair bundles. *Proc. R. Soc. Lond. Ser. B Biol. Sci.* **250**, 217–227 (1992).
24. N. Gavara, R. S. Chadwick, Noncontact microrheology at acoustic frequencies using frequency-modulated atomic force microscopy. *Nat. Methods* **7**, 650–654 (2010).
25. A. X. Cartagena-Rivera, C. M. Van Itallie, J. M. Anderson, R. S. Chadwick, Apical surface supracellular mechanical properties in polarized epithelium using noninvasive acoustic force spectroscopy. *Nat. Commun.* **8**, 1030 (2017).
26. P. K. Legan, V. A. Lukashkina, R. J. Goodyear, M. Kössl, I. J. Russell, G. P. Richardson, A targeted deletion in α-tectorin reveals that the tectorial membrane is required for the gain and timing of cochlear feedback. *Neuron* **28**, 273–285 (2000).
27. P. Hakizimana, W. E. Brownell, S. Jacob, A. Fridberger, Sound-induced length changes in outer hair cell stereocilia. *Nat. Commun.* **3**, 1094 (2012).
28. R. S. Chadwick, A. X. Cartagena-Rivera, Using noncontact AFM frequency shifts to determine stereocilia bundle stiffness and tension in the developing cochlear sensory epithelium. *AIP Conf. Proc.* **1703**, 030012 (2015).
29. H.-J. Butt, M. Jaschke, Calculation of thermal noise in atomic force microscopy. *Nanotechnology* **6**, 1 (1995).
30. A. J. Ricci, B. Kachar, J. Gale, S. M. Van Netten, Mechano-electrical transduction: New insights into old ideas. *J. Membr. Biol.* **209**, 71–88 (2006).
31. L. G. Tilney, D. J. Derosier, M. J. Mulroy, The organization of actin filaments in the stereocilia of cochlear hair cells. *J. Cell Biol.* **86**, 244–259 (1980).
32. F. Gittes, B. Mickey, J. Nettleton, J. Howard, Flexural rigidity of microtubules and actin filaments measured from thermal fluctuations in shape. *J. Cell Biol.* **120**, 923–934 (1993).
33. J. R. Meyers, R. B. MacDonald, A. Duggan, D. Lenzi, D. G. Standaert, J. T. Corwin, D. P. Corey, Lighting up the senses: FM1-43 loading of sensory cells through nonselective ion channels. *J. Neurosci.* **23**, 4054–4065 (2003).
34. M. Müller, K. von Hünerbein, S. Hoidis, J. W. T. Smolders, A physiological place–frequency map of the cochlea in the CBA/J mouse. *Hear. Res.* **202**, 63–73 (2005).
35. J. A. Kaltenbach, P. R. Falzarano, T. H. Simpson, Postnatal development of the hamster cochlea. II. Growth and differentiation of stereocilia bundles. *J. Comp. Neurol.* **350**, 187–198 (1994).
36. J.-H. Nam, A. W. Peng, A. J. Ricci, Underestimated sensitivity of mammalian cochlear hair cells due to splay between stereociliary columns. *Biophys. J.* **108**, 2633–2647 (2015).
37. K. D. Karavitaki, P. D. Niksch, D. P. Corey, Weak lateral coupling between stereocilia of mammalian cochlear hair cells requires new stimulus methods to study the biomechanics of hearing. *J. Acoust. Soc. Am.* **133**, 3509 (2013).
38. S. T. Smith, R. S. Chadwick, Simulation of the response of the inner hair cell stereocilia bundle to an acoustical stimulus. *PLOS ONE* **6**, e18161 (2011).

39. V. Bormuth, J. Barral, J.-F. Joanny, F. Jülicher, P. Martin, Transduction channels' gating can control friction on vibrating hair-cell bundles in the ear. *Proc. Natl. Acad. Sci. U.S.A.* **111**, 7185–7190 (2014).
40. J. Barral, F. Jülicher, P. Martin, Friction from transduction channels' gating affects spontaneous hair-bundle oscillations. *Biophys. J.* **114**, 425–436 (2018).
41. C. A. J. Putman, K. O. Van der Werf, B. G. De Grooth, N. F. Van Hulst, J. Greve, Tapping mode atomic force microscopy in liquid. *Appl. Phys. Lett.* **64**, 2454 (1994).
42. D. N. Furness, Y. Katori, B. Nirmal Kumar, C. M. Hackney, The dimensions and structural attachments of tip links in mammalian cochlear hair cells and the effects of exposure to different levels of extracellular calcium. *Neuroscience* **154**, 10–21 (2008).
43. J. Rueda, R. Cantos, D. J. Lim, Tectorial membrane-organ of Corti relationship during cochlear development. *Anat. Embryol.* **194**, 501–514 (1996).

Acknowledgments: We thank P. Diers for help on mice colony maintenance, K. Szarama and N. Gavara (Queen Mary University of London) for helpful discussions on AFM explant sample preparation and FM-AFM experiments, and E. Tyler (Medical Arts Design Section, NIH) for help with illustrations (Fig. 1). We acknowledge R. J. Morell (NIDCD) and the Genomics and Computational Biology Core facility with grant ZIC DC000086 as well as J. Chatel-Poujade (Institut Pasteur) for help with tail biopsies and PCR genotyping. We thank S. Smith (Howard University) and N. Gavara for critical reading and thoughtful comments on the manuscript. **Funding:** A.X.C.-R. and R.S.C. were supported by intramural funding of the Division of Intramural Research Program at the National Institute on Deafness and Other Communication Disorders with grant 1ZIADC00003322. S.L.G. and E.V. were supported by the European Commission (ERC-2011-ADG-294570). K.R. was supported by the NIDCD Genomics and Computational Biology Core facility with grant ZIC DC000086. **Ethics statement:** All animal care and procedures carried out in the NIH were approved by the Animal Care and Use Committee at NIH and complied with NIH guidelines for the care and use of animals. Animal experiments conducted at the Pasteur Institute were conducted in compliance with French and European regulations on protection of animals used for scientific purposes (project authorization number: 00274.03). **Author contributions:** A.X.C.-R., E.V., and R.S.C. conceived and designed the experiments. A.X.C.-R. performed the AFM and confocal fluorescence experiments on explants, carried out all the data analysis, and generated all the figures. S.L.G. generated the double-knockout mice. S.L.G and E.V. performed the SEM experiments. E.V. performed confocal fluorescence microscopy experiments on cryosections. K.R. and S.L.G. performed the tail biopsies and PCR genotyping. A.X.C.-R., E.V., and R.S.C. cowrote the article. All the authors discussed the results and reviewed the article. **Competing interests:** The authors declare that they have no competing interests. **Data and materials availability:** All data needed to evaluate the conclusions in the paper are present in the paper and/or the Supplementary Materials. Additional data supporting the findings and conclusions of this study are available from the corresponding author upon reasonable request. Correspondence and request for materials should be addressed to R.S.C. (chadwick@helix.nih.gov).

Submitted 25 April 2018
Accepted 10 January 2019
Published 20 February 2019
10.1126/sciadv.aat9934

Citation: A. X. Cartagena-Rivera, S. Le Gal, K. Richards, E. Verpy, R. S. Chadwick, Cochlear outer hair cell horizontal top connectors mediate mature stereocilia bundle mechanics. *Sci. Adv.* **5**, eaat9934 (2019).

ScienceAdvances

Cochlear outer hair cell horizontal top connectors mediate mature stereocilia bundle mechanics

Alexander X. Cartagena-Rivera, Sébastien Le Gal, Kerianne Richards, Elisabeth Verpy and Richard S. Chadwick

Sci Adv **5** (2), eaat9934.
DOI: 10.1126/sciadv.aat9934